JoT JOURNAL OF TURBULENCE

http://jot.iop.org/

Large-eddy simulation of bubbly turbulent shear flows†

Djamel Lakehal[1]‡, Brian L Smith[2] and Massimo Milelli[2]

[1] Institute of Energy Technology, ETH Zurich, ETH Zentrum/CLT, CH 8092 Zurich, Switzerland
[2] Thermal-Hydraulics Laboratory, Paul Scherrer Institute, CH 5232 Villigen PSI, Switzerland
E-mail: lakehal@iet.mavt.ethz.ch

Received 5 October 2001
Published 3 May 2002

Abstract. This paper reports on recent advances in the application of the large-eddy simulation (LES) approach to turbulent, vertical mixing layers containing bubbles at low void fraction. The method is based on the filtered multi-fluid equations derived from the application of a single component-weighted volume-averaging process. The subgrid-scale (SGS) modelling is based on the Smagorinsky kernel in both its original form and the dynamic procedure of Germano. Parameter studies have been undertaken to determine the effects of the ratio of the *cut-off* filter to the typical length scale characterizing the dispersed phase, the influence of the lift coefficient, the performance of the SGS models and the importance of inlet turbulence levels. A new model is proposed for possible bubble-induced turbulence modulation, in which the mixing length of the dispersed phase at the SGS is inferred dynamically from the resolved flow field. By averaging over times longer than the dynamic time scales of the turbulent fluctuations, mean quantities, including phase velocities and void fractions, are derived, which are then compared against experimental data. A critical discussion of the usefulness of LES approaches in this context is given. Overall, the LES approach shows considerable promise in regard to predicting mean quantities including phase velocities and void fractions.

PACS numbers: 47.27.Eq, 47.55.Kf

† This article was chosen from Selected Proceedings of the Second International Symposium on Turbulence and Shear Flow Phenomena (KTH-Stockholm, 27–9 June 2001) ed E Lindborg, A Johansson, J Eaton, J Humphrey, N Kasagi, M Leschziner and M Sommerfield.

‡ Author to whom any correspondence should be addressed.

 PII: S1468-5248(02)35598-X 1468-5248/02/000001+21$30.00

Contents

1. Introduction

Three-dimensional mixing of two-phase bubbly flows occurs in many industrial applications, including gas stirring of liquid metal ladles in several metallurgical processes, bubble-column mixers in chemical processing, and venting of vapour mixtures to liquid pools in nuclear reactors. Bubbly flows also play an important role in environmental processes, such as the aeration of lakes, mixing of stagnant water, and destratification of water reservoirs. For all these applications the basic need is to determine the currents induced by the evolving gaseous phase in the surrounding liquid, and the subsequent mixing and partition of energy, or species concentration, in the core flow.

The interface topology in this class of flow is intermittent to a considerable degree and also heterogeneous—compared, for example, with the simple situation of a single rising bubble or a falling liquid film. This explains why the prediction strategies must rely on a certain form of averaged transport equations with additional unclosed interfacial interaction terms. These are *smoothly* distributed over the computational domain since they are proportional to a continuous function known as the void fraction, reflecting the rate of occurrence of one phase within a defined control volume (or during a defined interval of time). The solution methods may be based on the Eulerian–Lagrangian approach or on the Eulerian–Eulerian variant, depending on the flow under consideration. In the Lagrangian reference frame, individual bubbles, or clouds of bubbles, are treated in a discrete way. The reference frame moves with the bubbles and the instantaneous location of each discrete entity is determined by reference to its origin and the time elapsed. In the Eulerian–Eulerian approach, also known as the *multi-fluid* or *interpenetrating media* formulation, the liquid and gas phases are treated as interpenetrating continuous media, each separately satisfying their own conservation and constitutive laws, and coupled by phase interaction relations. This method has the advantage that two-way coupling between phases can easily be represented, but does require the appropriate mass, momentum and energy exchanges between the phases to be readily quantified.

A key point in modelling bubbly flows is related to the representation of the local turbulence phenomena, and how these dictate the way the local exchanges take place in the mixture. Turbulence modulation due to the presence and motion of the bubbles is also to be expected, even at low void fractions. Until recently, most modelling strategies in this context have relied on extensions of single-phase turbulence models based on the Reynolds-averaged Navier–Stokes equations (RANS); see, for example, [1]–[4]. Models based on the RANS framework have generally proved disappointing in the multi-phase flow context, even in reproducing the global characteristics of the flow. But, even beyond this aspect, it is questionable whether the RANS concept is suitable for this class of flow since, by relying on time averaging, the models tend to filter out both the small-scale turbulence and the instantaneous interactions between the eddies and the dispersed phase. This is the reason why a multitude of models, known as *turbulent dispersion models*, have been advanced to approximate this two-way effect, in addition to closure laws for the Reynolds stresses within each phase. In practice, this idea was most often realized in terms of a superposition of shear-induced and bubble-induced stress tensors in the equations for the liquid phase; the latter being constructed on the basis of scaling arguments.

The necessity for a global strategy, dispensing with previous RANS-based approaches, is clearly evident. In the present work we explore the use of the LES method, in which the large-scale motions are solved directly and the smallest motions, including the interaction of the bubble motion with the surrounding turbulence, are represented in terms of subgrid models. The rationale behind the approach derives from the expectation that large-scale motions will interact strongly with the bubbles themselves, and will therefore be largely responsible for the macroscopic bubble motion, including dispersion, whereas the subgrid scales (SGSs) will be less important, affecting mainly the small-scale bubble oscillations. Consequently, the interfacial momentum forces will be accounted for at the resolved supergrid level only. The SGS turbulence modelling strategy is based on the Smagorinsky [5] kernel, both in its original form and via the dynamic procedure (DSM) of Germano *et al* [6], in which the non-resolved scales are approximated from the resolved velocity field. The SGS global dissipative effect, including the modulation induced by the dispersed phase, is modelled via a novel *hybrid* strategy, in which the typical length scale characterizing the dispersed phase is inferred dynamically from the resolved velocity field rather than involving the bubble diameter. This idea reflects the following physical mechanism: the rate of turbulence dissipation at the SGS level due to the liquid- and bubble-induced fluctuations is entirely dictated by the motion of the large-scale energetic eddies.

In a first step, before investigating bubble-driven flows (plumes), the test case selected here to pursue these ideas is the vertical bubbly shear layer studied experimentally by Roig *et al* [7]. One advantage of opting for this case study is that the flow may be considered as being statistically two dimensional, which helps in conducting sensitivity studies to determine the influence of the ratio of the cut-off filter to the typical length scale characterizing the dispersed phase, the effect of varying the lift coefficient, the predictive performance of specific physical and SGS models, and the effect of initial turbulence levels. A second advantage is the fact that bubbles are of small, uniform diameter (typically 3 mm), and void fractions are small (≈2–3%), so that bubble–bubble interaction effects are negligible.

2. Governing equations and subgrid-scale modelling

2.1. The two-fluid approach: basic concept

Describing the motion of multi-phase flow systems in terms of model transport equations is fundamentally subject to a certain degree of approximation due to the phase averaging required by the presence of more than one phase. In the present context, use is made of the *multi-fluid* formulation to describe the simultaneous presence of various phases at each point in the

mixture. Without exploring this concept in detail, it suffices to say that it has been presented in various forms† (e.g. [8]–[13]). In all cases, a rigorous formalism requires the two-phase continuum equations to be derived by averaging over length or time scales large compared to those characteristic of the dispersed phase motions, but small compared to those characterizing the mean flow (Λ and Θ).

The starting point is the exact, or microscopic, instantaneous equations governing each phase evolving in the system. This preliminary *microscale description* involves the smallest possible length and time scales (λ and θ) compatible with the continuum formulation [14]. The standard conservation laws for each phase can thus formally be written using the phase indicator function $\chi(\boldsymbol{x}, t)$ at time t and point x defined by

$$\chi^k(\boldsymbol{x}, t) = \begin{cases} 1 & \text{for } x \in k \\ 0 & \text{otherwise} \end{cases} \tag{1}$$

to demarcate volumes occupied by each phase k. In the absence of heat and mass transfer, the balance equations for each phase are multiplied by χ (see, for example, [11]):

$$\chi^k \frac{\partial}{\partial t}(\rho^k) + \chi^k \frac{\partial}{\partial x_j}(\rho^k u_j^k) = 0 \tag{2}$$

$$\chi^k \frac{\partial}{\partial t}(\rho^k u_i^k) + \chi^k \frac{\partial}{\partial x_j}(\rho^k u_i^k u_j^k) = \chi^k \frac{\partial}{\partial x_j}\Pi_{ij}^k + \chi^k \rho^k g_i \tag{3}$$

where ρ^k is the phase density, g denotes gravity, and the superscript k refers either to the dispersed phase ($k = d$) or to the continuous phase ($k = c$). The phase net stress, composed of the pressure contribution and the viscous stress, σ_{ij}^k, is defined by

$$\Pi_{ij}^k = -p^k \delta_{ij} + \sigma_{ij}^k. \tag{4}$$

At this stage, the above system of equations only reflects the presence of multiple components within the system. The inter-penetration of the phases and the subsequent interfacial interactions stem from applying *phase averaging* to the pre-averaged microscopic equations (2) and (3). Whether this is performed over time, space or an ensemble, phase averaging always gives rise to extra unclosed quantities that require modelling. This *macroscale description* of the flow is precisely what leads to the instantaneous *phase-averaged multi-fluid equations* describing each component as a continuum, regardless of whether the flow regime is laminar or turbulent. But again, proper model derivation requires the averaging to be performed over intermediate length or time scales larger than λ and θ and smaller than Λ and Θ.

Further, the direct numerical simulation (DNS) of this system of equations should resolve most of the relevant turbulent scales, but since this is not realistic in practice, a further averaging of the *phase averaged multi-fluid equations* can then be performed, leading to averaged turbulent quantities for each phase, analogous to Reynolds stresses. This additional flow decomposition, which we shall refer to as *turbulence averaging*, may either be a non-weighted time average or a Favre-weighted average based on α^k, the volume fraction. This is rigorously defined as the ratio of the volume of component k in an arbitrary small region to the total volume of the region in question, i.e. $\alpha^k \equiv \langle \chi^k \rangle$. Once adopted, Reynolds averaging ($f = \overline{f} + f'$) generates extra second-order and third-order correlations involving variable fluctuations α' and f', which also require appropriate modelling. Note that this complication can easily be avoided by the use of Favre-weighted averaging [15].

The present formulation aims at unifying the micro-scale and macro-scale descriptions discussed above by adopting a single *component-weighted volume averaging* procedure, which directly leads to a system of *filtered two-fluid equations*. The main difference compared with

† We exclude reference to the variants based on ensemble averaging.

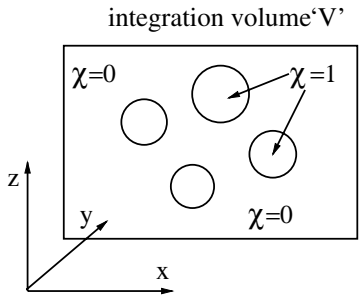

Figure 1. Definition of the control volume for phase averaging.

earlier formulations is the use of a unique large spatial filter instead of doubling the averaging procedure, e.g. 'ensemble' then 'space' or 'space' then 'space'. This is synonymous to the LES approach in which scales larger than the space filter (represented in this case by the grid size) are solved directly, and the smaller SGSs are modelled.

2.2. The filtered two-fluid equations

Instead of resorting to the usual volume averaging procedure [8, 9, 12], the present work relies on translating this into a generalized convolution product as was first applied to multiphase flows by Bataille [14]. The topological equation reflecting the material derivative of χ^k following the interface can be written as

$$\frac{\mathrm{D}\chi^{\mathrm{k}}}{\mathrm{Dt}} = \frac{\partial \chi^k}{\partial t} + u_j^k \frac{\partial \chi^k}{\partial x_j} = 0. \tag{5}$$

By use of the above equation, the system of instantaneous equations (2) and (3) can be recast into a more convenient form:

$$\frac{\partial}{\partial t}(\chi^k \rho^k) + \frac{\partial}{\partial x_j}(\chi^k \rho^k u_j^k) = 0 \tag{6}$$

$$\frac{\partial}{\partial t}(\chi^k \rho^k u_i^k) + \frac{\partial}{\partial x_j}(\chi^k \rho^k u_i^k u_j^k) = \chi^k \frac{\partial}{\partial x_j}\Pi_{ij}^k + \chi^k \rho^k g_i. \tag{7}$$

For flow systems involving immiscible continuous phases, we start the derivation by assuming the domain of the flow (D) to be composed of control volumes (V) containing both fluids, each occupying a volumetric proportion equal to V^k/V (cf figure 1). For obvious reasons this volume has to be larger than the characteristic length scale of the dispersed phase λ^d, denoting the bubble diameter and/or spacing. The volume averaging procedure employed here derives from the filtering process utilized within the LES framework, conventionally defined by

$$\overline{f(\boldsymbol{x})} = \int_D G(\boldsymbol{x} - \boldsymbol{x}'; \Delta)\, f(\boldsymbol{x}')\, \mathrm{d}\boldsymbol{x}' \tag{8}$$

where $G(\boldsymbol{x} - \boldsymbol{x}'; \Delta)$ represents an appropriate spatial filter defined such that

$$\int_D G(\mathbf{x} - \mathbf{x}'; \Delta)\, \mathrm{d}\boldsymbol{x}' = 1 \tag{9}$$

with Δ being the filter width. For the sake of simplicity, the convolution product represented by equation (8) is denoted by

$$\overline{f(\boldsymbol{x})} = G \otimes f(\boldsymbol{x}). \tag{10}$$

The wavelength of the smallest scale retained by the filtering operation corresponds to the filter width defined here as $\Delta = (\Delta x \Delta y \Delta z)^{1/3}$, where Δx denotes the cell size in the streamwise direction, etc. Within the multi-fluid approach it is conceptually desirable to identify each phase k by defining a quantity reflecting the averaged volumetric fraction of that phase within a volume V, i.e. the void fraction in the present context:

$$\alpha^k(\boldsymbol{x}) = \overline{\chi^k(\boldsymbol{x})} = G \otimes \chi^k(\boldsymbol{x}). \tag{11}$$

The *filtered multi-fluid equations* are obtained by resorting to the *component-weighted volume-averaging* process†, in which

$$\tilde{f}^k = \frac{\overline{\chi^k f^k}}{\overline{\chi^k}} \equiv \frac{G \otimes f^k(\boldsymbol{x})\,\chi^k(\boldsymbol{x})}{G \otimes \chi^k(\boldsymbol{x})}. \tag{12}$$

Without explicitly assuming commutativity of the filtering operation with respect to the differential operators (in contrast to LES for single-phase flows), applying now the above variable definition to equations (6) and (7) results in the filtered multi-fluid equations:

$$\frac{\partial}{\partial t}(\alpha^k \rho^k) + \frac{\partial}{\partial x_j}(\alpha^k \rho^k \tilde{u}_j^k) = 0, \qquad \sum \alpha^k = 1, \tag{13}$$

$$\frac{\partial}{\partial t}(\alpha^k \rho^k \tilde{u}_i^k) + \frac{\partial}{\partial x_j}(\alpha^k \rho^k \tilde{u}_i^k \tilde{u}_j^k) = \frac{\partial}{\partial x_j}\alpha^k[\tilde{\Pi}_{ij}^k - \tau_{ij}^k] + \alpha^k \rho^k g_i + \mathcal{M}^k. \tag{14}$$

The above set of equations has the same form as those derived by Tran [16] and Lance *et al* [17]. Note, too, that use was made of the conventional decomposition of the stress tensor into resolved and SGS components, i.e.

$$\tau_{ij}^k = \rho^k(\widetilde{u_i u_j}^k - \tilde{u}_i{}^k \tilde{u}_j{}^k). \tag{15}$$

The SGS tensor τ_{ij}^k needs to be modelled in terms of determinable (i.e. filtered) quantities for each phase. The last term in the filtered momentum equations is a pure interfacial force resulting from filtering the diffusive flux $\Pi_{ij}^k \partial_j(\chi^k)$:

$$\mathcal{M}^k \equiv G \otimes \Pi_{ij}^k n_j^k \delta(\boldsymbol{x} - \boldsymbol{x}_I) \tag{16}$$

where n_j^k stands for the normal unit vector pointing outward of phase k, and δ for the Dirac distribution identifying the interface location with $\boldsymbol{x}_I$. Indeed, the first term on the right-hand side of equation (7) can be written as

$$\chi^k \frac{\partial}{\partial x_j}\Pi_{ij}^k = \frac{\partial}{\partial x_j}\chi^k \Pi_{ij}^k + \Pi_{ij}^k n_j^k \delta(\boldsymbol{x} - \boldsymbol{x}_I) \tag{17}$$

noting that

$$\frac{\partial \chi^k}{\partial x_j} = -n_j^k \frac{\partial \chi^k}{\partial n_j^k} = -n_j^k \delta(\boldsymbol{x} - \boldsymbol{x}_I). \tag{18}$$

More important to note is that, in contrast to the filtered single-phase equations, a conceptual restriction arising in the present approach is that the cut-off filter Δ should strictly be larger‡ than the length scale characteristic of the dispersed phase λ^d. The dilemma posed is in

† This is similar to Favre averaging in which the weighting function is the density ρ. In connection with this, if the flow is compressible on each side of the interface, the density is no longer constant, in which case the above defined filter should be phrased as a *component and density weighted volume averaging* process, and expressed as $\tilde{f}^k = \overline{\rho^k \chi^k f^k}/\overline{\rho^k \chi^k}$.

‡ Both the filter width Δ and the length scale characteristic of the dispersed phase λ^d should be defined such that $\lambda < \lambda^d < \Delta < \Lambda$.

determining an appropriate choice of the ratio Δ/λ^d providing a sufficient large-scale resolution while not violating this restriction. The non-resolved SGSs, $u_i'^k = u_i^k - \tilde{u_i}^k$, represent the portion of flow details of wavelength smaller than Δ smoothed out by applying equation (12); these scales include possible bubble-induced fluctuations. The conjuncture suggests that the SGS motion of the continuous phase, in particular, may be affected by bubble-induced agitation, and as such it needs to be represented by the SGS model.

2.3. Interfacial momentum forces

The simultaneous presence of the phases also imposes an approximation for the interfacial term $\mathcal{M}^k$, reflecting the global force exerted by the phases on each other, but at the supergrid level. Let us assume that each control volume V forming the flow domain D is populated by n_b bubbles of volume V_b. If G is taken as a top-hat or boxcar filter of width $\Delta \equiv V^{1/3}$ and height $1/\Delta$, we may write the interfacial force $\mathcal{M}^k$ as

$$G \otimes \Pi_{ij}^k n_j^k \delta(\boldsymbol{x} - \boldsymbol{x}_I) \equiv \frac{1}{V} \sum_{l=1}^{n_b} \int_S \Pi_{ij}^k \, n_j^k \, \mathrm{d}S \tag{19}$$

where S is the surface of the bubble. If we now explicitly separate the filtered stress divergence term $\alpha^k \partial_j(\tilde{\Pi_{ij}^k})$ from the first term on the right-hand side of equation (14), and use the Gauss theorem to transform its volume integral into a surface integral, equation (19) may be transformed into a filtered interfacial force of the form

$$\mathcal{M}'^k = \alpha^k \int_S [\Pi_{ij}^k - \tilde{\Pi_{ij}^k}] \, n_j^k \, \mathrm{d}S \tag{20}$$

where the integral represents the forces per unit dispersed phase volume. In the particular case of a single bubble rising in a quiescent, pure fluid, the force exerted by the continuous phase on the bubble encompasses the drag, lift, virtual (or added) mass and Basset history forces, i.e. F_d, F_l, F_a and F_h. The Basset history contribution is often neglected. Assuming a dilute-loading limit, the filtered interfacial force given by equation (20) can be equally formulated:

$$\mathcal{M}'^d = -\mathcal{M}'^c = \alpha^d (\tilde{F_d} + \tilde{F_l} + \tilde{F_a}). \tag{21}$$

The closure laws for these three components are well documented in the literature [10, 12, 18, 19, 20]. In the present case, however, each filtered contribution is naturally expressed in terms of resolved velocities $\tilde{u_j}^k$. For example, invoking small-to-negligible SGS effects on the global drag force, $\tilde{F_d}$ can be approximated by

$$\tilde{F_d} \approx \frac{3}{4} \frac{C_d^*}{d_b} \rho^c \, |\tilde{\boldsymbol{u}}^c - \tilde{\boldsymbol{u}}^d| \, (\tilde{\boldsymbol{u}}^c - \tilde{\boldsymbol{u}}^d) \tag{22}$$

where ρ^c denotes the density of the continuous phase, d_b the bubble diameter and C_d^* the modified drag coefficient which should deviate slightly from the *true* (valid for a non-deformable sphere immersed in a Stokes flow) coefficient C_d. Beyond the Stokes regime, C_d can be determined from

$$C_d = \frac{24}{Re_d} (1 + 0.1 Re_d^{0.75}); \qquad Re_d = \frac{d_b |\tilde{\boldsymbol{u}}^c - \tilde{\boldsymbol{u}}^d|}{\nu^c}. \tag{23}$$

The modified drag coefficient C_d^* is proposed to account for the SGS effects, but in the absence of experimental or firmer numerical evidence its value was taken equal to that of C_d determined from equation (23). The filtered virtual mass force, which appears because the bubble acceleration also requires acceleration of the surrounding fluid, is also approximated by

$$\tilde{F_a} \approx \rho^c \, C_a^* \left(\frac{\mathrm{D}\tilde{\mathrm{u}}_\mathrm{i}^\mathrm{d}}{\mathrm{Dt}} - \frac{\mathrm{D}\tilde{\mathrm{u}}_\mathrm{i}^\mathrm{c}}{\mathrm{Dt}} \right) \tag{24}$$

in which the value of the modified added mass coefficient C_a^* is taken here equal to that (exact) for a single sphere rising in an infinite fluid [21], i.e. $C_a = 0.5$, assuming dilute suspensions of spheres in a fluid.

The filtered lift force acting on the bubble is expressed herein as follows:

$$\tilde{F}_l \approx \rho^c \, C_L^* \, \epsilon_{ijk} \, (\tilde{u}_j^c - \tilde{u}_j^d) \, \tilde{\omega}_j^c \tag{25}$$

where $\tilde{\omega}_j^c$ stands for the liquid filtered vorticity and ϵ_{ijk} denotes the permutation tensor. Again, the modified lift coefficient C_L^* is supposed to account for the SGS effects. Note that there is no generally accepted value of the lift coefficient for a swarm of bubbles, although $0.25 < C_L < 0.5$ is most often used. More than the other two terms, the flow is extremely sensitive to the lift force, affecting most the distribution of the phases, essentially because of the presence of the vorticity in equation (25). The value assigned to its coefficient may therefore play a key role in the simulation. A sensitivity study to this parameter has been carried out and results are presented in this paper.

2.4. Subgrid scale modelling

The dissipative scales of motion, including the bubble-induced ones for the continuous phase, are not resolved and require as such a model reproducing energy transfer from the resolved scales. The SGS stress tensor τ_{ij}^k in equation (15) is approximated by applying the eddy viscosity concept, in which the deviatoric part is linearly related to the resolved rate of strain tensor $\tilde{S}_{ij}^k$ according to

$$\tau_{ij}^k = -2\mu_{sgs}^k \tilde{S}_{ij}^k + \tfrac{1}{3}\delta_{ij}\tau_{kk}^k; \qquad \tilde{S}_{ij}^k = \frac{1}{2}\left(\frac{\partial \tilde{u}_i^k}{\partial x_j} + \frac{\partial \tilde{u}_j^k}{\partial x_i}\right). \tag{26}$$

Unlike in compressible flows, the trace of τ_{ij}^k is often embodied into the modified pressure. The coefficient of proportionality, μ_{sgs}^k, is known as the turbulent viscosity. Assuming that the dissipative scales are in equilibrium, μ_{sgs} may be scaled in a conventional way via a length scale and a time scale. According to Smagorinsky [5], the turbulent viscosity can be written as

$$\mu_{sgs} = (C_s \Delta)^2 \rho |\tilde{S}|; \qquad |\tilde{S}| = \sqrt{2\tilde{S}_{ij}\,\tilde{S}_{ij}}. \tag{27}$$

More specifically, in the multi-fluid context, the presence of the dispersed phase is known to contribute (together with the unresolved scales of motion) to the process of energy removal (or dissipation, $\varepsilon_{sgs} \equiv \mu_{sgs}^3/\lambda^4$) from the resolved scales of the liquid phase [22]. In the context of equation (26), this two-way coupling effect can be interpreted as a modulation of μ_{sgs} by its bubble-induced counterpart, μ^d. By assuming the dispersed phase to follow the liquid motion at the SGS level, Tran [16] developed a model for μ^d in which it was assumed that the velocity scales of the smallest resolved motion and the dispersed phase were identical, which is probably true for micro-bubbles. The effective viscosity for the continuous phase $\mu_{sgs}^c + \mu_{bub}^c$ was of the form

$$\mu_{eff}^c = \mu_{sgs}^c \left[1 + C_f \alpha^d 6\pi \frac{d_b \mu^c}{\Delta \mu_{sgs}^c}\right]^{1/3}, \tag{28}$$

in which μ^c is the molecular viscosity and $C_f = 0.17$ is a model constant. The model is in effect grossly dissipative since the coefficient C_f is assigned a fixed value.

Milelli *et al* [23] advanced another idea according to which it is the mixing length of the dispersed phase, λ^d, that may be comparable to the smallest resolved scales, since the bubbles are known to have a tendency to break the eddies into scales of similar size [22]. Support for this argument can be found in the scale-similarity principle of Bardina *et al* [24], which states that

the smallest resolved scales are similar to the largest modelled ones; the latter in the present context are the bubbles themselves. The eddy viscosity can then be scaled as the superposition of shear-induced and bubble-induced SGS energy dissipation mechanisms:

$$\mu^c_{eff} = (C_s\Delta)^2\rho^c|\tilde{S}^c_{ij}| + (C_s\Delta)\rho^c\alpha^d|\tilde{\boldsymbol{u}}^c - \tilde{\boldsymbol{u}}^d| \tag{29}$$

where we have set λ^d equal to $(C_s\Delta)$ and the velocity scale of the dispersed phase equal to the slip velocity, $|\tilde{\boldsymbol{u}}^c - \tilde{\boldsymbol{u}}^d|$. Note that, in an earlier RANS-based work, Sato *et al* [2] incorporated the bubble diameter d_b as a length scale together with the slip velocity to account for the same effect. In the LES context, however, both Sato's [2] proposal and the above model (29) with constant C_s would make the SGS model grossly dissipative. It would therefore make more sense to use equation (29) in connection with the DSM approach so as to accommodate the mutual transfer of dissipated momentum between the phases: from the bubbles to the surrounding fluid whenever $C_s > 0$, and vice versa whenever $C_s < 0$. Note also that the difference between the proposed idea and that of Tran [16] is in the scaling arguments adopted: the similarity between the resolved scales and the dispersed phase in terms of velocity scale can only apply to micro-bubbles, which indeed tend to follow the liquid motion because of strong drag effects.

For the present application the standard SGS model (26) was employed both with the Smagorinsky constant $C_s = 0.12$ and using the DSM approach of Germano *et al* [6]. A top-hat filter was employed and the ratio of the test filter to the grid filter was taken equal to two. And, as written above, the bubble-induced dissipation model (29) was combined with the DSM approach only.

3. Simulation set-up

The experimental facility of [7], shown schematically in figure 2, consists of a vertical square-channel air–water loop. The convergent channel is divided at the bottom into two parts by a splitter plate, each side being supplied independently by a mixture of bubbles and water at specified rates.

In the sensitivity part of the investigation, the flow was calculated in two dimensions, taking the risk of violating the LES method which conceptually is three dimensional. The three-dimensional computational domain was deliberately truncated compared with the experiment (30 cm width, 60 cm height and 4 cm depth), and slip boundary conditions were imposed on the lateral planes. This measure was found to be equivalent to extending the domain and imposing non-slip wall conditions using the wall function approach of Werner and Wengle [25]. On top of the domain a constant pressure boundary condition was imposed. At the bottom, the phases were injected with the profiles measured at the end of the splitter plate (at $x = -1$ cm), a level corresponding to the inlet boundary in the present simulations. Two sets of grids were employed for the two-dimensional sensitivity calculations. The finest one consisted of 100×200 nodes, and the coarse one of 30×40 nodes. The three-dimensional grid, consisting of 200,000 nodes, was uniformly distributed ($\Delta x = 3.5$ mm, $\Delta y = 3$ mm, $\Delta z = 4$ mm) to maintain a constant filter width over the entire domain. The inlet void fraction ($\alpha^d = 1.9\%$, with bubbles of 3 mm diameter), liquid and gas mean velocities (0.22 m s^{-1} in the slow channel and 0.54 m s^{-1} in the fast channel) and the rms velocity profiles were all taken from the experiment. Both two- and three-dimensional calculations were carried out for about 5000 time steps (with $\Delta t = 0.001$ s) to reach statistically steady-state solutions. The calculations were performed using a structured, multi-block, multi-grid, finite-volume code employing a fully co-located storage arrangement. A second-order central differencing scheme was used for the spatial discretization, and a second-order, fully implicit, backward differencing scheme for the time marching. The solution was iterated to convergence using a pressure-correction approach.

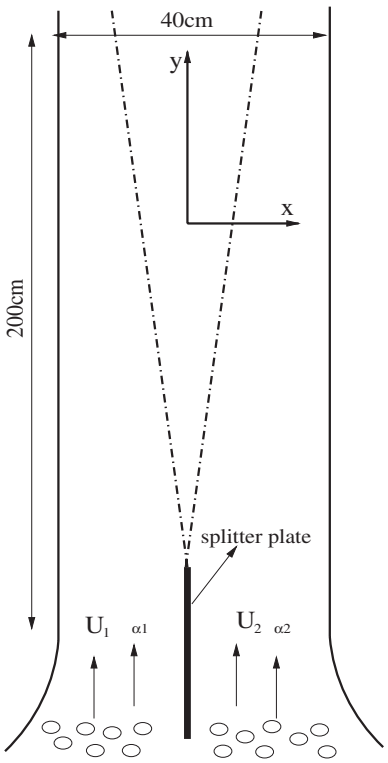

Figure 2. Experimental set-up (from [7]).

4. Two-dimensional simulations: parametric study

4.1. On the value of the lift coefficient and cut-off filter width

The implications on the results of both the filter width Δ and the value assigned to the modified lift coefficient C_L^* were examined within the context of the standard Smagorinsky SGS model with $C_s = 0.12$. In the dispersed-phase context, the typical length scale could either be the bubble diameter, $\lambda^d \equiv d_b$, or the inter-bubble spacing, $\lambda^d \equiv I_b$. These are, in fact, related by the void fraction α (assuming spherical bubbles) via $\alpha \approx (d_b/I_b)^3$. This implies that considering the impact of the ratio Δ/λ^d makes more sense if λ^d could be represented by the inter-bubble spacing. For the sake of clarity, however, the results are presented in what follows based on Δ/d_b.

Results for the u_{rms} distributions obtained with varying C_L^* for the coarse and fine grids are compared against experimental data in figure 3. They clearly indicate that, independently of the value assigned to C_L^*, rigorous resolution requires the cut-off filter Δ to be comparable to the bubble size. With the coarse grid, the rms velocities were generally grossly exaggerated and the void fraction and velocity profiles were rather flat (results not shown here). More precise indications of the effect of varying the lift coefficient can be seen in the context of figure 4, comparing the void fraction distributions at two elevations using the fine grid. But figure 3 already suggests that, without the lift force, the simulation misrepresents the lateral spreading of the plume at the expense of a strong oscillation in the rms magnitude. Figure 4 confirms this result through the ragged profiles of void fraction for $C_L^* = 0$, but it also shows overpredicted peaks for $C_L^* = 0.5$. Judging from this figure in particular, one is tempted to conclude that $C_L^* = 0.25$ is the best compromise for this class of flow, in conformity with the recommendations of Drew and Lahey [21].

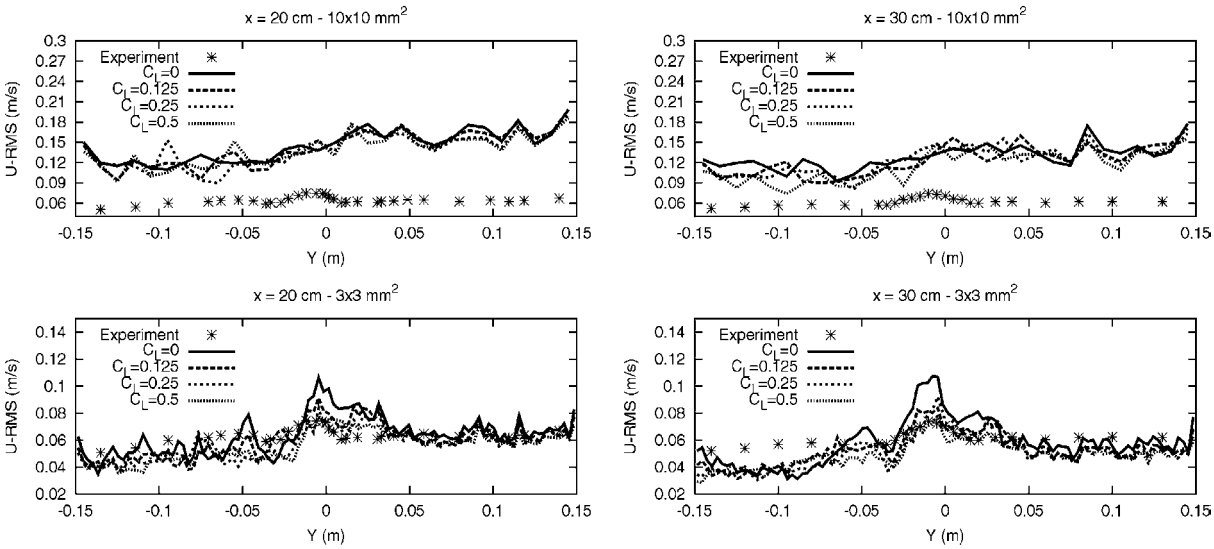

Figure 3. u_{rms} distributions for the coarse and fine meshes. Calculations with variable C_L^* and standard SGS model with $C_s = 0.12$.

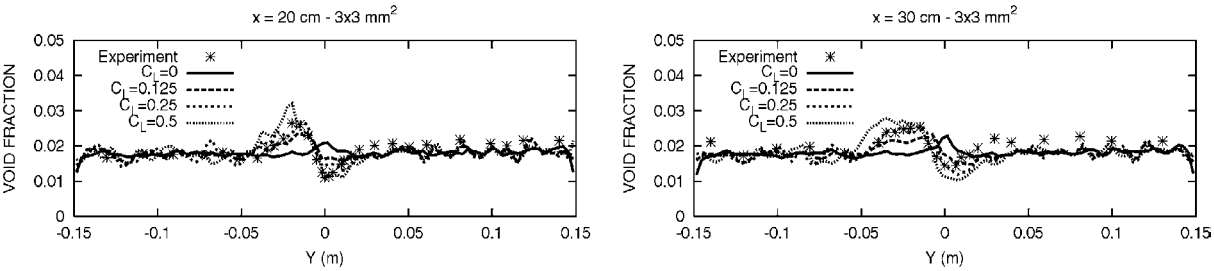

Figure 4. Void fraction distributions for the fine mesh ($\Delta/d_b = 1.5$). Calculations with variable C_L^* and standard SGS model with $C_s = 0.12$.

In summary, it appears that, with this level of void fraction (1.9%), and with a cut-off length scale significantly larger than the characteristic length of the dispersed phase ($\Delta/d_b = 3.33$), the simulation cannot capture all the important scales involved in the flow; best results are obtained with $\Delta/d_b = 1.5$. On the other hand, it is likely that, in the absence of bubbles, a rigorous LES of this flow would require an equal grid resolution owing to the low void fraction (1.9% only). But, apart from that, a large ratio of Δ/λ^d will leave an unresolved gap of intermediate length scales interacting with the bubbles still needing to be modelled.

A further optimization exercise, in which $\Delta/d_b = 1.6$ and $C_L^* = 0.25$, led to the results displayed in figure 5. There it is shown that both the velocity distributions and void fraction distributions compare well with the experiment, but not the rms values away from the mixing zone. This points to two plausible reasons: either the three dimensionality of the flow has an appreciable *global* effect on the fluctuating field, in which case a two-dimensional idealization is restrictive, or the bubble-induced fluctuations at the large-scale level in weak shear regions are not well captured.

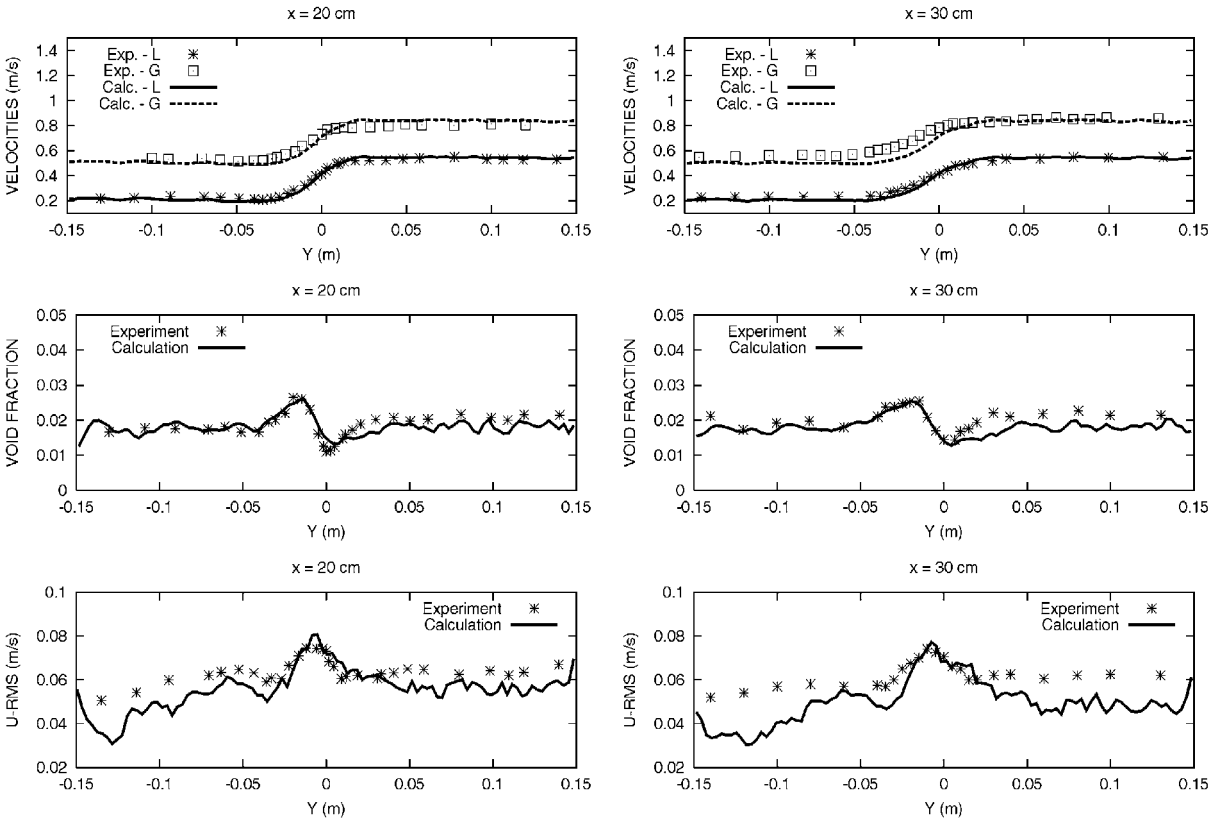

Figure 5. Distributions of mean velocities, void fraction and u_{rms}. Calculations (two dimensional) with $\Delta/d_b = 1.6$ and $C_L^* = 0.25$ and standard SGS model with $C_s = 0.12$.

4.2. On the SGS modelling

The predictive performance of the employed SGS models is discussed within the context of figure 6 comparing the liquid velocity fluctuations with the experiments. Immediately after the injection location, at $x = 6$ cm, the standard SGS model with constant C_s delivers an overpredicted level of u_{rms} compared with the DSM. The panel also shows that the performance of the DSM is better in the shear region, and in the rapid channel, than in the slow channel away from the mixing zone. The tendency is somewhat inverted at the next location, in the sense that results of the standard SGS model are the closest to the experiment. The misrepresentation of the rms values away from the shear region is equally shared by both models; the possible explanations for this behaviour have already been described.

The reason why, at $x = 6$ cm, the velocity fluctuations are more pronounced in the standard model is probably due to the flow there still being affected by the proximity of the injection, in which case the actual C_s level is well above the value of 0.12 (it has actually a space average of 0.147). This naturally leads to a pronounced effective viscosity that attenuates further the fluctuating field compared with the standard model. Looking at the next location ($x = 20$ cm) reveals that the level of u_{rms} is generally underpredicted, more with the use of the DSM than by the standard model. This is a misleading result since at that location the values of C_s were, on average, smaller than 0.12. At $x = 30$ cm, where the averaged C_s value was found to converge towards 0.121, the standard and modified SGS models deliver almost the same result (results not shown).

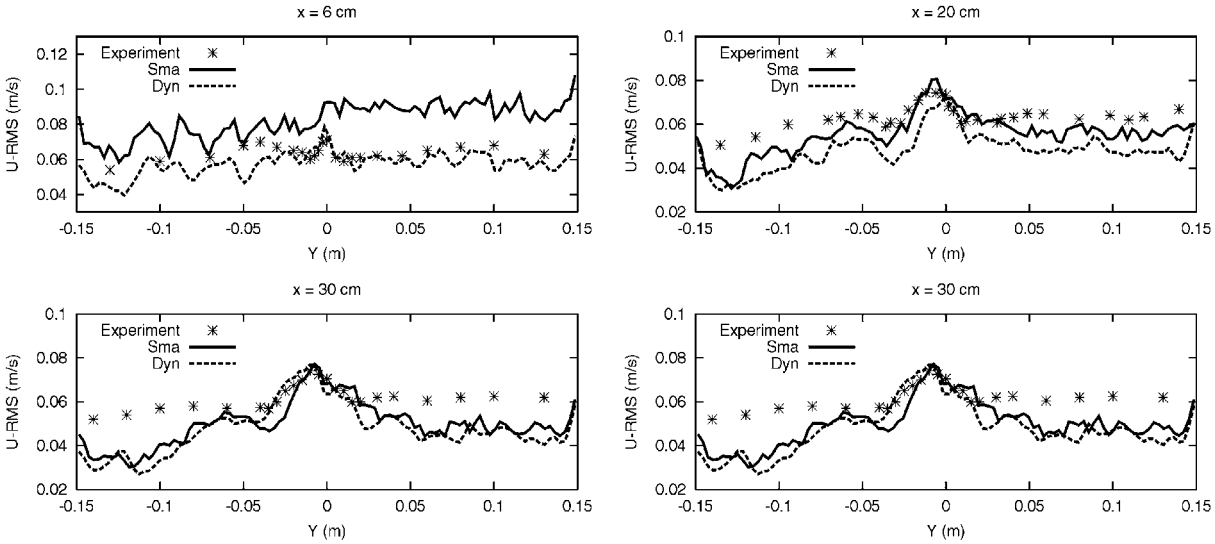

Figure 6. u_{rms} distributions obtained with the standard and DSM SGS models. Calculations with $\Delta/d_b = 1.6$ and $C_L^* = 0.25$.

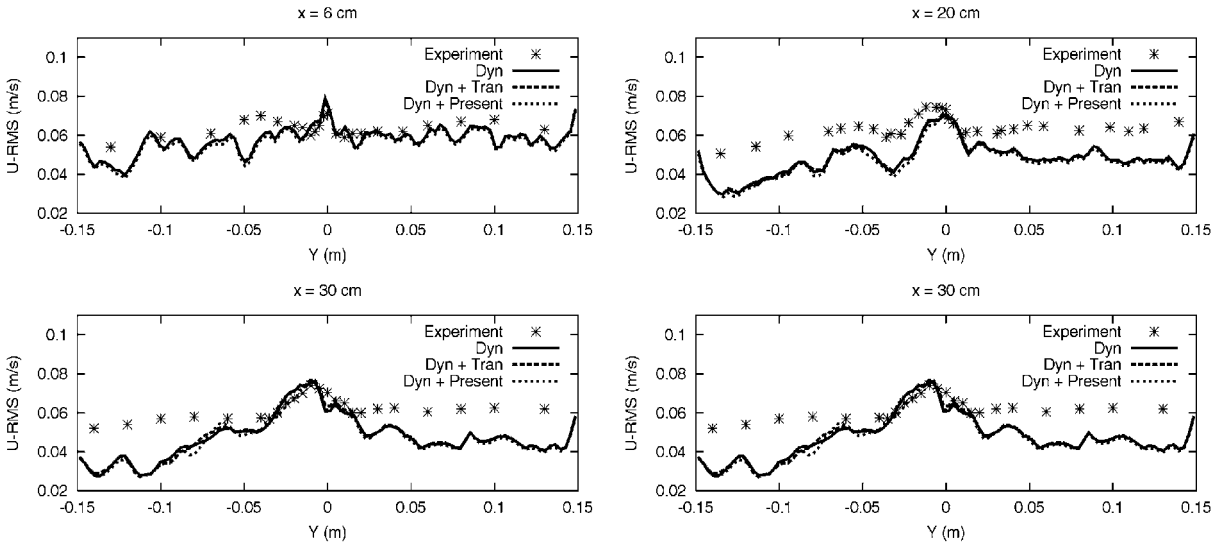

Figure 7. u_{rms} distributions obtained with various DSM-based models. Calculations with $\Delta/d_b = 1.6$ and $C_L^* = 0.25$.

Comparison of the time-averaged liquid and gas velocity and volume fraction α^d distributions delivered by the DSM approach, combined with the Tran model (28) or the present one (29) for bubble-induced dissipation, revealed that these quantities are not sensitive to either of the two models (results not included here). Overall, these predicted quantities agreed very well with the experiment. The u_{rms} distributions plotted in figure 7 are in line with the conclusion drawn from the previous analysis: i.e. the fluctuating field perceives the effect of promoting the eddy viscosity as a secondary effect only. When looking at figure 8, which shows the distributions of the ratio μ_{eff}/μ, the previous remark may seem somewhat misleading, since the effective viscosity appears now to be enhanced (by a factor of 2 at both $x = 20$ and $x = 30$ cm),

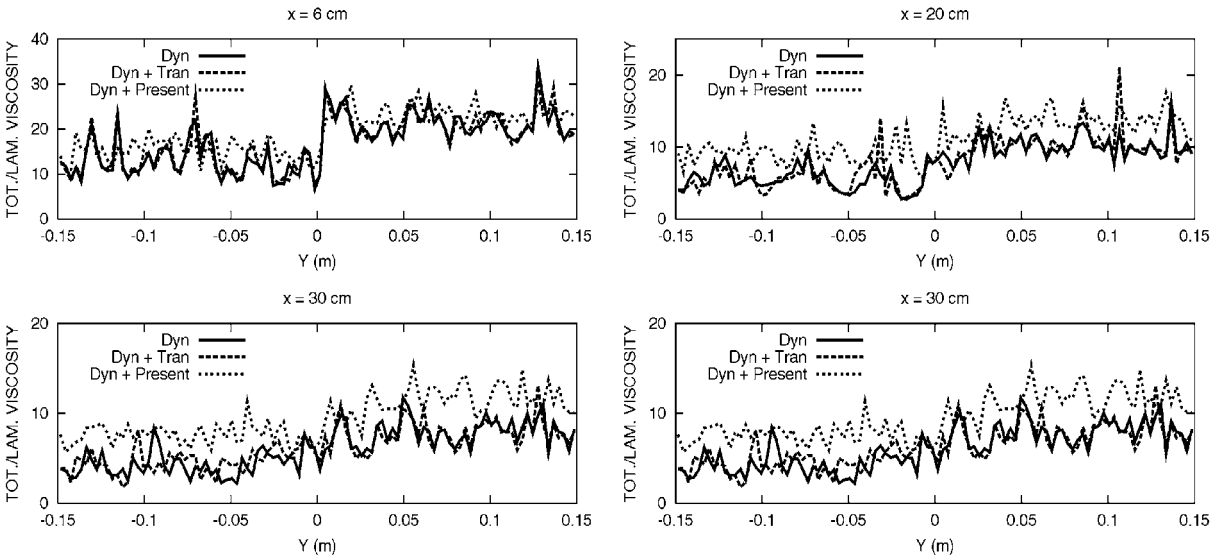

Figure 8. Distributions of μ_{eff}/μ obtained with various DSM-based models. Calculations with $\Delta/d_b = 1.6$ and $C_L^* = 0.25$.

particularly away from the mixing zone. But obviously, the shear stresses are important only in the regions where appreciable velocity gradients occur. In summary then, in the context of an idealized two-dimensional simulation, it seems that representing the bubble-induced rms velocity field in terms of a purely shear-type model is not sufficient. However, a final conclusion cannot be drawn without looking at three-dimensional calculations. Also, close inspection of figure 8 raises an additional point: at both elevations around the mixing zone the magnitudes of μ_{eff}/μ are comparable to those delivered by the DSM alone. This could *tentatively* be interpreted as the capacity of the proposed model to allow the shear stress to be solely dictated by the strength of the rate of strain $\tilde{S}_{ij}$, wherever appropriate. Finally, it is worth noting from figure 8 that the Tran [16] model seems to have negligible impact compared with the one proposed here, which is not surprising (from a formulation point of view, at least) since the presence of the power 1/3 in equation (28) tends to smooth this term out.

5. Three-dimensional simulations

5.1. On the flow structure

Results are presented from three-dimensional simulations with various SGS model combinations, and are compared against the data of Roig *et al* [7]. However, prior to that, it is perhaps worth recapitulating the main conclusions drawn from the sensitivity analysis: for the level of void fraction employed here, the optimum grid concentration has to be such that the ratio of the cut-off filter to the bubble diameter is ≈1.5; a good compromise can be obtained with a lift coefficient of $C_L^* = 0.25$; the Smagorinsky model performs quite well and gives results comparable to those of the dynamic procedure of Germano; modifying the SGS model to account for bubble-induced effects has not been conclusive.

The one-dimensional streamwise turbulent energy spectrum, taken at a point located in the mixing zone, is displayed in figure 9. The spectrum exhibits a broad range turbulence, with a slope oscillating between the single-phase $-5/3$ and the two-phase $-8/3$ power laws in the inertial sub-range. Previous experimental studies have actually attributed the more dissipative

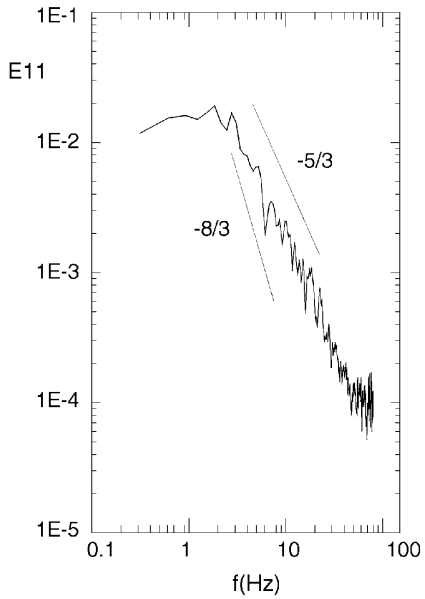

Figure 9. One-dimensional streamwise turbulent kinetic energy spectrum.

spectrum to the presence of the dispersed phase, this being responsible for eddy disintegration. The present result indicates, however, that at this low void fraction the effect of the bubbles on the surrounding turbulence may be negligible.

Snapshots of the velocity vectors taken in the middle of the domain at two time steps ($t = 5$ and $t = 7$ s) are shown in figure 10. The flow clearly exhibits the low speed and high speed regions. Note too, the formation of large-scale motions visible in the slow channel in particular. The mixing zone between the two channels, identified by a high shear, appears to be oscillating along the flow direction. Figure 11 shows two snapshots of volume fraction distributions taken in the mid-plane of the domain. The structure of the flow observed in the previous figure is also reproduced by these contours. The figure clearly shows the smooth interpenetration of the phases, without a clear distinction of the interface. More important to note is the separation between two distinct flow regions: close to the injection the bubbly phase is still sparsely distributed with a clear presence of the small scales, whereas far downstream these structures seem to be smoothed out in favour of the large-scale motions. The oscillation of the mixing zone at the centre of the domain is also clearly shown.

5.2. Averaged and rms quantities: two dimensional versus three dimensional calculations

Two- and three-dimensional calculations are discussed within the context of figures 12 and 13, comparing the time-averaged streamwise velocities and void fractions, respectively. Figure 12 shows almost no differences between the two sets of calculations. It also indicates that the LES results do reproduce fairly well the self-preserving behaviour of the plume, in accordance with the data. This supports the idea that the flow is statistically two dimensional and can therefore be simulated as such. Note in particular that, at $x = 40$ cm in the slow channel, the predictions are underestimated. In fact, the results have often been observed to begin systematically to deviate from the measurements for $x > 40$ cm, in particular in the slow (left) channel. This was attributed by the authors of the experiment to the lack of precision in measuring the inlet profile of the void fraction in that channel. The distribution of void fractions reported in figure 13 is consistent with the discussion concerning the mean velocities in the sense that only minor

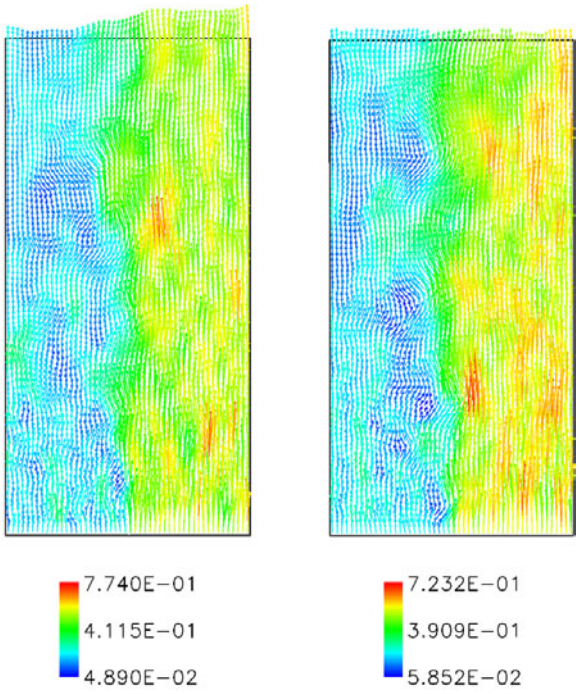

Figure 10. Instantaneous resolved velocity vectors in the mid-plane of the domain.

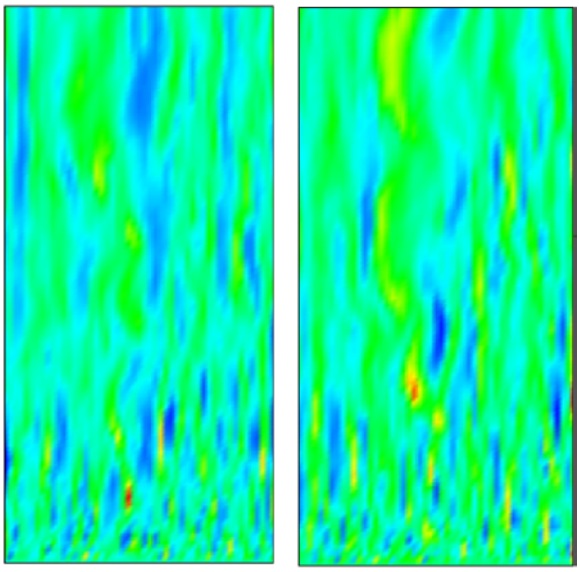

Figure 11. Contours of volume fraction distribution in the mid-plane.

differences are perceptible in the two simulations. Also, the peaks at $x = 6$ cm, where the flow is still affected by the proximity of the injection, are misrepresented by the same amount. Again, one notes that the agreement between the simulations and measurements is rather good, but slight deviations start to appear further downstream.

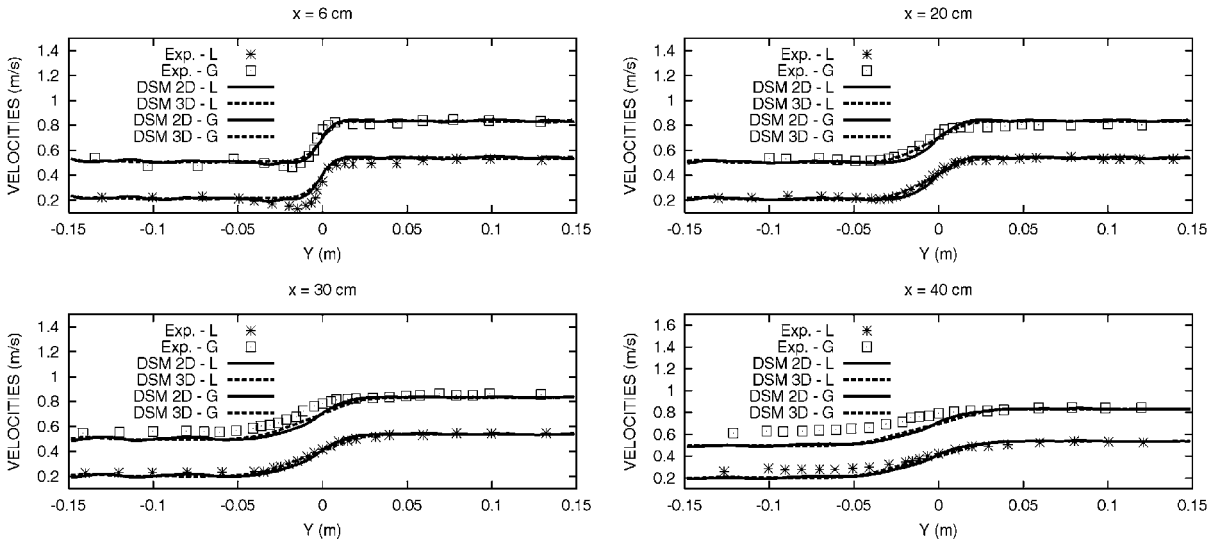

Figure 12. Two- and three-dimensional time-averaged liquid and gas velocities.

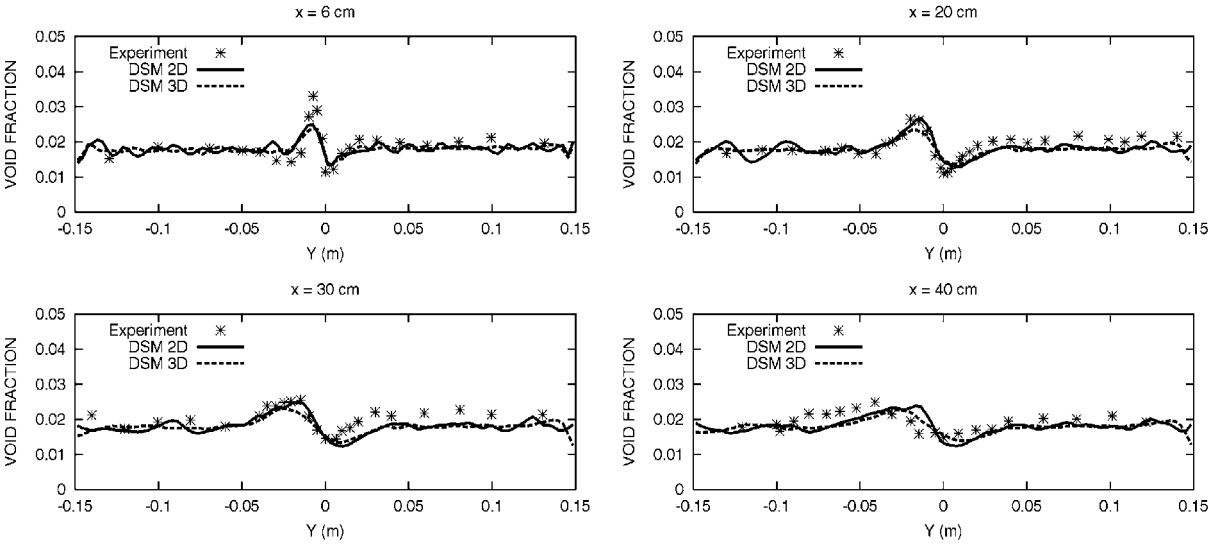

Figure 13. Two- and three-dimensional time-averaged void fractions.

5.3. On the SGS modelling

The rms streamwise velocities resulting from the standard SGS model and the DSM variant combined with equation (29) are plotted in figure 14 at two cross-flow locations. The figure includes results of both two- and three-dimensional simulations; the latter are spatially averaged over each cross-flow plane. The upper two panels compare the two- and three-dimensional simulations obtained from the standard SGS model with $C_s = 0.12$. Unlike the time-averaged quantities, the panels show a surprising underestimate of the rms velocities in the three-dimensional calculation, but more in the slow channel (left) than in the high speed one. This result also supports what has been observed previously in connection with time-averaged predictions, in that there is evidence for an uncertainty regarding the experimental data for the slow channel. It may also be true that the dissipative behaviour of the standard model affects the results in the low-speed region more than in the high-speed one. The lower two panels

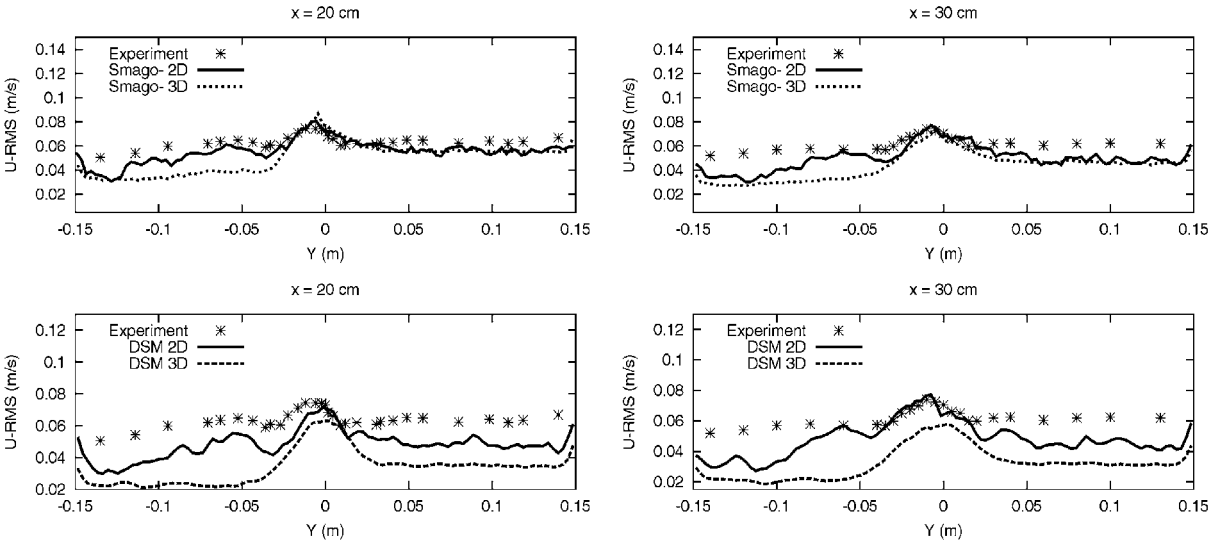

Figure 14. Two- and three-dimensional u_{rms} velocities obtained with two SGS models.

indicate that the more elaborate DSM model grossly underpredicts this turbulence quantity, in particular away from the zone of strong shear. The comparison indicates that results are actually worse when the flow is simulated in three dimensions. Again, the fact that the difference is more pronounced in the slow channel suggests that the experimental inflow conditions are not well reproduced, in particular the profile of void fraction and turbulence intensity. The other source of error may be related to the truncated size of the computational domain, in particular in the third direction which was taken too narrow, and the boundary conditions applied at the outer boundaries. Results (not included here) of the length scale obtained with the dynamic procedure employed in three dimensions show that the parameter C_s is strongly overpredicted compared to the Smagorinsky value, while in two dimensions its value was always close to 0.12.

The predictive performance of both SGS models is discussed within the context of figure 15, displaying both time-averaged and rms quantities obtained in three dimensions. The models result in almost identical time-averaged velocities and volume fractions, in accordance with the data. In line with previous discussions, the DSM approach of Germano underpredicts the fluctuating velocity field compared to the standard model, in particular away from the mixing zone. The fact that results of both SGS models significantly deviate from the data reinforces the conclusion that turbulence is more sensitive to the computational details, including the size of the domain and the inflow conditions, than to the SGS modelling. The new proposal for bubble-induced turbulence modulation seems not to produce the expected results, probably because the dispersed phase in this case is very dilute, so that its role is minimized in the turbulence dissipation mechanism at the SGS level. The turbulence energy spectrum shown in figure 9 has already shown evidence for little impact of the dispersed phase on the liquid. On the other hand, because the computational domain was not sufficiently dimensioned, the large scales were not adequately resolved, in which case the DSM model combined with the model for bubble-induced dissipation turns out to be more dissipative than the standard model. In this case, modifying the eddy viscosity via equation (29) is counterproductive. This issue is clearly not yet conclusive and needs further clarification through a systematic sensitivity study focusing on the influence of the computational domain.

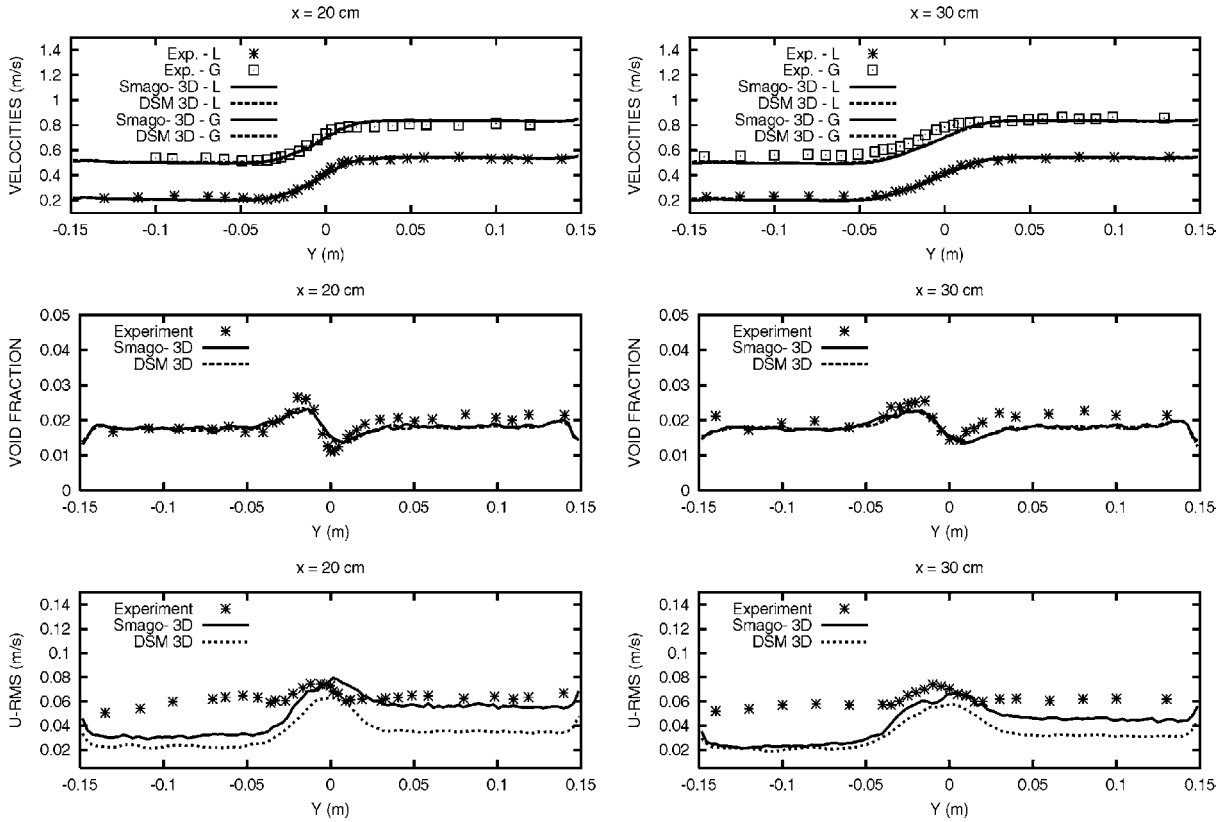

Figure 15. Time-averaged velocity and void fraction profiles and rms quantities obtained with two SGS models.

6. Concluding remarks

LES simulations of an isothermal, highly turbulent, vertical shear layer laden with bubbles at very low void fraction has been performed. The method is based on the filtered multi-fluid equations derived by the application of a single component-weighted volume-averaging process. The SGS modelling is based on the Smagorinsky kernel in both its original form and in the form of the dynamic procedure of Germano, in which the length scale is inferred from the resolved scale motion. The test case was investigated experimentally by Roig *et al* [7]. Although the experiment is well documented, most of the available data are time-averaged quantities, and little information is given on turbulence statistics that could be utilized for validating the proposed model for bubble-induced turbulence.

Parameter studies have been undertaken to determine the effects of the ratio of the cut-off filter to the length scale characteristic of the dispersed phase, the influence of the lift coefficient, the performance of the SGS models, and the importance of inlet turbulence levels. Two-dimensional calculations have revealed that, for an inlet void fraction of about 2%, the optimum grid concentration has to be such that the ratio of the cut-off filter to the bubble diameter is ≈1.5. A good compromise can be obtained with a lift coefficient of $C_L^* = 0.25$ and the Smagorinsky model performs quite well and gives results comparable to those of the dynamic procedure of Germano.

The simulations have also shown that the flow is statistically two dimensional; two- and three-dimensional time-averaged quantities were virtually the same. Three-dimensional simulations have also confirmed that the dynamic approach of Germano does not perform

better than the Smagorinsky model. The DSM strategy has even proved disappointing in predicting turbulence intensities, most probably because the dimensions of the computational domain were not adequate. Modifying the SGS model to account for bubble-induced dissipation did not bring the expected results, probably because at low void fractions the bubbles only have a minor influence on the turbulence level in the liquid, as revealed by the energy power spectrum. It is suspected that modifying the shear-induced dissipation may result in a counter effect if the large-scale motions are not rigorously resolved. More important to note is that, in contrast to single-phase flow experiments (including DNS), there is an inherent difficulty in measuring turbulence quantities in two-phase flows, making direct meaningful comparison with the calculations difficult. In this respect, the data taken for validation in this work present obvious uncertainties. Finally, this novel LES strategy for multi-fluid components, supposed to surpass the conventional RANS approach, needs to be further validated before applying it to flows where the overall motion is buoyancy driven, such as in bubble plumes.

Acknowledgments

The authors wish to thank Professors G Yadigaroglu and M Lance for their valuable suggestions and comments. The first author wishes to express his gratitude to Professor S Elghobashi for his useful ideas and to C Narayanan for the extended discussions we have had while the manuscript was in preparation.

References

[1] Lopez de Bertodano M, Lahey R T and Jones O C 1994 Development of a k–ε model for bubbly two-phase flows *J. Fluids Eng.* **116** 128–34
[2] Sato Y, Sadatomi I and Sekoguchi I 1981 Momentum and heat transfer in two-phase bubbly flow-I *J. Multiphase Flow* **7** 167–77
[3] Smith B L and Milelli M 1998 An investigation of confined bubble plumes *3rd Int. Conf. on Multi-Phase Flow ICMF'98 (Lyon)* (CD ROM) paper 641
[4] Carrica P M, Drew D, Bonetto F and Lahey R T 1999 A polydisperse model for bubbly two-phase flow around surface ships *J. Multiphase Flow* **25** 257–305
[5] Smagorinsky J 1963 General circulation experiments with the primitive equations I the basic experiment *Mon. Weather Rev.* **91** 99–165
[6] Germano M, Piomelli U, Moin P and Cabot W H 1991 A dynamic subgrid-scale eddy viscosity model *Phys. Fluids* **3** 1760–5
[7] Roig V, Suzanne C and Masbernat L 1997 Experimental investigation of a turbulent bubbly mixing layer *J. Multiphase Flow* **24** 35–54
[8] Ishii M 1975 *Thermo-Fluid Dynamics Theory of Two-Phase Flow* (Paris: Eyrolles)
[9] Delhaye J M and Achard J L 1977 On the use of averaging two-phase flow modelling *Thermal and Hydraulic Aspects of Reactor Safety vol 1: Light Water Reactors* ed S G Bankoff (New York: ASME) pp289–332
[10] Banerjee S and Chan M C 1980 Separated flow models-I *J. Multiphase Flow* **6** 1–24
[11] Delhaye J M 1987 Fundamentals of time-varying two-phase flow formulation *Proc. Int. Seminar Transient Phenomena in Multiphase Flow (Dubrovnik)* ed N H Afgan (New York: Hemisphere) pp 24–30
[12] Lahey R T and Drew D A 1988 The three-dimensional time and volume averaged conservation equations of two-phase flows *Adv. Nucl. Sci. Technol.* **20** 1–69
[13] Besnard D C and Harlow F H 1988 Turbulence in multiphase flow *J. Multiphase Flow* **14** 679–99
[14] Bataille J 1981 Averaged field equations for multiphase flows *DOE Report No* GEOFLO/9 Brown University Division of Engineering, Providence, RI
[15] Elghobashi S 1994 On predicting particle-laden flows *Appl. Sci. Res.* **52** 309–29
[16] Tran M L 1997 Modélisation instationnaire de la distribution spatiale des phases dans les ecoulements diphasiques en régimes à bulles *Doctoral Thesis* University Claude Bernard Lyon
[17] Lance M, Marie J and Bataille J 1999 Turbulence in bubbly blow: from experiments to numerical modelling *Proc. 2nd Int. Symp. on Two-Phase Flow Modelling and Experimentation (Pisa, Italy)* ed G P Celata, P di Marco and R K Shah (Pisa: ETS) pp 23–6

[18] Auton T R, Hunt J C R and Prud'homme M The force exterted on a body in inviscid unsteady non-uniform rotational flow *J. Fluid Mech.* **197** 241–57
[19] Smith B L 1998 On the modelling of a bubble plume in a liquid pool *Appl. Math. Modelling* **22** 773–97
[20] Zhang D Z and Prosperetti A 1994 Ensemble phase-averaged equations for bubbly flows *Phys. Fluids* **8** 2956–70
[21] Drew D A and Lahey R T 1987 The virtual mass and lift force on a sphere in rotating and straining inviscid flow *J. Multiphase Flow* **13** 113–21
[22] Lance M Bataille J 1991 Turbulence in the liquid phase of a uniform bubbly air–water flow *J. Fluid Mech.* **222** 95–118
[23] Milelli M, Smith B L and Lakehal D 2001 Large-eddy simulation of turbulent shear flows laden with bubbles *Direct and Large-Eddy Simulation IV* ed B J Geurts, R Friedrich and O Metais (Amsterdam: Kluwer Academic) pp 461–70
[24] Bardina J, Ferziger J H and Reynolds W C 1980 Improved subgrid models for large eddy simulation *AIAA paper* 80–1358
[25] Werner H and Wengle H 1989 Large-eddy simulation of flow over and around a cube in a plate channel *Proc. TSF8* ed Durst *et al* (Berlin: Springer) pp 155–68